STUDIA UBB CHEMIA, LXX, 4, 2025 (p. 275-292)
(RECOMMENDED CITATION)
DOI:10.24193/subbchem.2025.4.16

HYDRAULIC MODELING AND OPTIMIZATION OF THE OIL GATHERING NETWORK IN THE PERIPHERAL FIELD RAMA–RAA NORTH, HASSI MESSAOUD (ALGERIA)

Ourdia AMZAL[a], Ahmed Salah Eddine MEDDOUR[a], Farid SOUAS[a*], Radia AKSOUH[a], Abdelhamid SAFRI[a]

ABSTRACT. This study presents the hydraulic modeling and optimization of the RAMA and RAA crude oil gathering network in Algeria's Hassi Messaoud oil field to enhance production efficiency and ensure stable field performance. A digital network model was developed using PIPESIM to simulate multiphase flow behavior from the wellheads to the Early Production Facility (EPF). The model calibration showed strong agreement between simulated and measured pressures, with deviations below 7%, confirming its reliability. Simulation results revealed several oversized flowlines with velocities below the recommended 1–5 m/s range and an undersized line (MFD BEKEN) exhibiting excessive velocities and pressure losses above 0.85 bar/km. To address these issues, the impact of integrating 11 new wells was evaluated, showing increase in line and manifold pressures. An optimization study was subsequently conducted by adjusting pipeline diameters and adding new flowlines in compliance with API design standards. The optimized configuration improved velocity distribution and reduced erosion risks, ensuring safer and more efficient network operation across the RAMA–RAA fields.

Keywords: *crude oil, flow behavior, hydraulic modeling, PIPESIM, RAMA–RAA fields, pipeline optimization.*

INTRODUCTION

Crude oil remains the dominant source of global energy, contributing approximately 37% of the world's total energy supply [1]. It plays a critical role in economic growth and industrial development, serving as the base for

[a] *LEGHYD Laboratory, Faculty of Civil Engineering, University of Science and Technology Houari Boumediene (USTHB), Bab Ezzouar, Alger, Algeria*
* *Corresponding author: fa.souas@gmail.com, farid.souas@usthb.edu.dz*

producing transportation fuels and a wide range of petrochemical products such as solvents, polymers, and intermediates [2]. Despite global efforts toward energy diversification, crude oil will continue to be an essential raw material in the foreseeable future. Light crude oils, such as Algeria's Saharan blend, are highly valued due to their low density, low sulfur and asphaltene content, and low viscosity, which make them relatively easier to transport.

Algeria is a key oil and gas producer with vast hydrocarbon reserves that are central to its national economy. Most of the country's petroleum resources are located in the southeastern Saharan region, particularly in large fields such as Hassi Messaoud. The oil and gas sector is dominated by the national company Sonatrach, which is responsible for both exploration and production. In an effort to boost overall output, Sonatrach has expanded operations to nearby satellite fields, including the RAMA-RAA field. However, the exploitation of this field presents operational challenges due to the long distances between wells and surface treatment facilities. Crude oil from RAMA-RAA is transported to the recently developed RAMA-2 Early Production Facilities (EPF) for initial processing and stabilization.

Nevertheless, several issues persist throughout the production and transportation chain. One of the most critical concerns is the deposition of asphaltenes and other heavy components, which can occur in various parts of the system, including near-wellbore regions, tubing, separators, and pipelines [3]. Recent studies on Algerian crude oils have also highlighted complex flow behavior driven by compositional variability and aging effects, particularly the distinctions between fresh crude and sludge deposits, which further complicate transportation and handling [4–6].

Crude oil is a complex mixture of hydrocarbons including aromatics, resins, and asphaltenes, resulting in non-Newtonian flow behavior under certain conditions. These suspended particles increase the risk of fouling and deposition along infrastructure, reducing energy efficiency and increasing operational costs [7]. Transporting crude oil through pipelines, especially over long distances, is particularly affected by changes in temperature, pressure, and composition. To better understand and mitigate these challenges, numerous researchers have studied the flow behavior of non-Newtonian fluids in different pipeline configurations. For example, Das et al. [8] investigated non-Newtonian flow through bends, while Trallero [9] focused on oil–water flow in horizontal pipes. Hansen [10] developed phenomenological models for multiphase flow in gravity separators, and Bannwart [11] explored core annular oil–water flow regimes. Bandyopadhyay and Das [12] proposed empirical correlations for pressure drop and flow resistance in different pipeline components. In addition, Rudman and Blackburn [13] applied direct numerical simulation (DNS) methods

to analyze the transport of non-Newtonian fluids, offering valuable insights into turbulent flow dynamics and supporting the design of more efficient pipeline systems.

The primary objective of this study is to develop and calibrate a reliable hydraulic model of the RAMA–RAA oil gathering network in Hassi Messaoud (Algeria) using PIPESIM, in order to identify operational inefficiencies and propose optimized pipeline configurations. This work is crucial for improving flow assurance, reducing pressure losses and erosion risks, and ensuring safe, stable, and efficient production. The optimized network serves as a practical framework for future well integration and development planning, contributing to enhanced field performance and long-term asset integrity.

This study contributes a calibrated hydraulic model of the RAMA–RAA gathering system and applies an integrated calibration–optimization workflow to diagnose velocity imbalance, evaluate erosion risk, and propose diameter and routing modifications tailored to long-distance multiphase networks.

RESULTS AND DISCUSSION

After developing the gathering network model, flow simulations were performed in PIPESIM to evaluate the hydraulic behavior of the system from the wellheads to the EPF. This analysis provided a clear overview of the flow regimes and helped identify sections prone to excessive pressure losses, corrosion, or erosion.

Model calibration was then conducted to ensure agreement between simulated and measured data. The process aimed to minimize the deviation between the measured pressure (Ppm) and the simulated pressure (Ppc), following the criterion:

$$Relative\ deviation = \frac{|Ppm - Ppc|}{Ppm} \leq 7\,\% \qquad (1)$$

The 7% acceptance threshold was selected as a conservative limit consistent with typical field gauge uncertainty and standard practice in preliminary network-model calibration.

Parameter tuning primarily involved adjusting the gas–oil ratio, pipe roughness, and the choice of flow correlation. The Beggs & Brill correlation [14] provided the best match between calculated and observed pressures. Figure 1 illustrates the calibration results, showing that all relative deviations between measured and simulated pressures are within the acceptable 7% range, confirming that the developed network model is well matched and accurately represents actual field conditions.

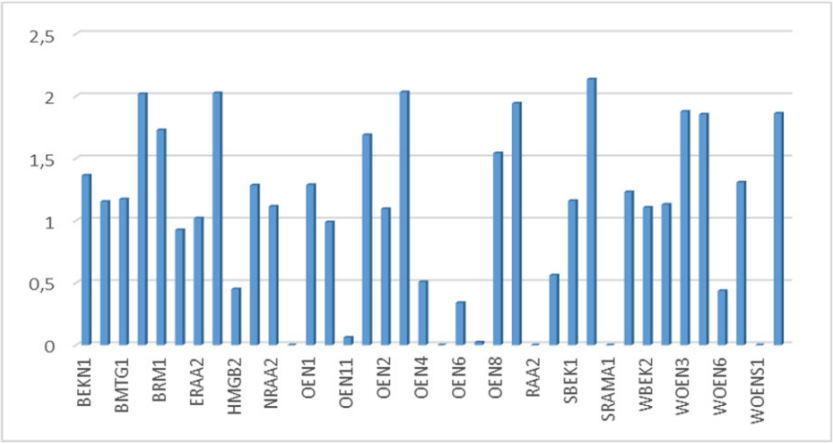

Figure 1. Model calibration result

Table 1. Results of the simulation of the existing network

Start	Gradient P (bar/km)	Mixture velocity Vm [1-5] m/s
JCT OEN	0.6	0.52
MFD BEKN	1.14	8.86
MFD OEN-M1	0.51	0.73
MFD OEN-M4	1.64	0.07
MFD OEN-M5	0.3	0.94
BEKN-1	0.93	0.09
BMTG-1	1.253	0.31
BMTG-2	2.038	0.83
ERAA-2	0.786	0.51
HMGB-2	0.783	0.81
NRAA-1	2	0.03
NRAA-2	0.044	0.14
OEN-1	11.80	0.69
OEN-10	0.337	0.06
OEN-11	0.665	0.98
OEN-12	0.495	0.68
OEN-6	0.563	0.82
OEN-7	0.4	0.66
OEN-9	0.337	0.97
RAA-5	0.948	0.5
SBEK-1	1.475	0.75
SOEN-1	1.395	0.03
WOEN-4	1.350	0.35
WOEN-7	12.500	0.49
ZMD-1	1.075	0.04

The calibrated model was subsequently used to analyze the hydraulic performance of the existing network. The results, summarized in Table 1, indicate that several flowlines are oversized as reflected by flow velocities below the recommended range of 1–5m/s, whereas the MFD BEKN line exhibits velocities exceeding acceptable limits, suggesting undersizing. In addition, many wells display pressure gradients greater than 0.85 bar/km, implying excessive head losses and potential operational inefficiencies. Overall, the simulation demonstrates that although the network performs satisfactorily, certain sections would benefit from resizing or optimization to improve flow distribution and minimize the risks of erosion or deposition.

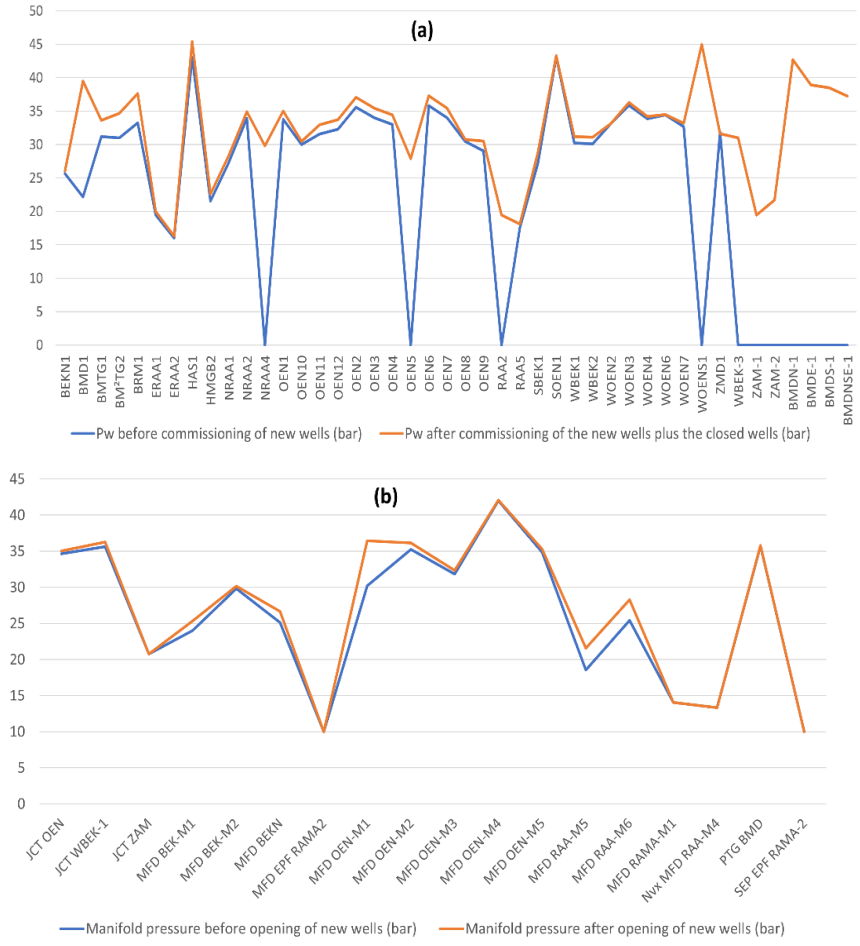

Figure 2. Comparison between current pressures and those after commissioning of new wells for (a) flowlines and (b) manifolds

In order to address the problem of oversized and undersized flowlines, additional wells were opened, including NRAA-4, OEN-5, RAA-5, and WOENS-1. Moreover, new wells currently under drilling — BMDE-1, BMDN-1, BMDS-1, and BMDNSE-1 — were considered in the simulation. The production parameters of BMD-1 were assumed to represent these new wells, with estimated values of Q = 10 m³/h, gas-oil ratio (GOR) = 250 sm³/sm³, and temperature = 26°C. In addition, the wells WBEK-3, ZAM-1, and ZAM-2 were included with the following estimated parameters:

– WBEK-3: Q = 8 m³/h, GOR = 200 sm³/sm³, T = 28°C
– ZAM-1: Q = 7 m³/h, GOR = 100 sm³/sm³, T = 45°C
– ZAM-2: Q = 10 m³/h, GOR = 120 sm³/sm³, T = 30°C

The parameters for future wells were estimated from analog wells in the same reservoir units and from historical production of the most representative existing producer (BMD-1). These values were provided by the operating company (EP SONATRACH) as planning assumptions.

Figure 2a presents the comparison between the current flowline pressures and those obtained after the commissioning of the new wells (BMDE-1, BMDN-1, BMDS-1, BMDNSE-1, ZAM-1, WBEK-3, ZAM-2). The analysis indicates that the flowline pressures were readjusted following the start-up of these wells, demonstrating an adaptation of the network to the evolving production conditions of the field. Figure 2b shows the comparison between current and post-commissioning manifold pressures. The simulation results reveal noticeable variations in manifold pressures after the integration of the new wells. Overall, it can be concluded that the commissioning of additional wells led to an increase in pipeline pressures for several existing producers. This rise in Pp may negatively affect the production performance of some wells, highlighting the need for network optimization to maintain stable and efficient operations.

To assess the impact of commissioning new wells on the RAMA and RAA gathering network, a new simulation scenario was developed, focusing on the analysis of mixture flow velocities. The Erosion Velocity Ratio (EVR), defined as the ratio between the actual flow velocity and the critical erosion velocity, was calculated to evaluate the risk of erosion. According to industry standards, the EVR value should remain below 70% to avoid potential erosion problems. An EVR threshold of 0.7 was adopted as a conservative screening limit commonly used in industry erosion-risk assessments (e.g., API RP 14E guidelines [15]).

The simulation of the RAMA–RAA gathering system after the commissioning of the 11 new wells showed that 33 flowlines are oversized (highlighted in yellow in Table 2) and three pipelines are undersized (highlighted in red in Table 2). Based on these findings, an optimization study was carried

out to adjust the line diameters and, where necessary, to propose the installation of additional pipelines. These modifications aim to ensure that the network complies with API design standards.

Table 2. Analysis of mixture velocity results

Name	System pressure loss (bar)	Mixture velocity at inlet (m/s)	Mixture velocity at outlet (m/s)	Maximum erosion velocity ratio (%)
BEKN-1	0.93	0.08	0.09	0.87
BMD-1	3.80	1.65	1.98	18.27
BMDE-1	3.21	0.72	0.87	8.60
BMDN-1	7.01	0.65	0.87	8.60
BMDS-1	2.80	0.74	0.87	8.60
BMDSE-1	1.57	0.78	0.87	8.59
BMTG-1	3.82	0.23	0.28	3.44
BMTG-2	4.88	0.60	0.76	7.84
BRM-1	2.41	0.82	0.95	11.10
ERAA-1	0.42	1.06	1.11	9.67
ERAA-2	2.26	0.43	0.53	5.05
HAS-1	20.03	0.04	0.06	0.98
HMGB-2	1.85	0.66	0.77	9.53
JCT OEN_MFD OEN-M3	2.78	0.45	0.49	5.92
JCT WBEK-1_MFD BEK-M1	11.60	0.60	0.97	9.08
JCT ZAM_MFD RAMA-M1	6.70	1.67	2.44	22.71
MFD BEK-M1_MFD EPF RAMA2	14.02	3.27	7.59	47.70
MFD BEK-M2_MFD BEK-M1	5.77	1.92	2.38	20.94
MFD BEKN_MFD EPF RAMA2	15.10	3.96	9.55	62.29
MFD OEN-M1_MFD BEKN	5.09	0.56	0.69	7.50
MFD OEN-M2_MFD BEK-M1	11.22	2.76	4.05	40.26
MFD OEN-M3_MFD BEKN	6.74	2.22	2.80	28.57
MFD OEN-M4_JCT OEN	7.36	0.05	0.06	1.00
MFD OEN-M5_MFD OEN-M3	3.00	0.82	0.90	11.05
MFD RAA-M5_Nvx MFD RAA-M4	5.19	0.54	0.73	8.03
MFD RAA-M6_MFD RAA-M5	6.98	0.13	0.17	3.36
MFD RAMA-M1_MFD EPF RAMA2	4.04	1.09	1.49	11.92
NRAA-1	0.45	0.03	0.03	0.59
NRAA-2	0.17	0.13	0.14	3.07
NRAA4	4.43	0.05	0.06	1.17
Nvx MFD RAA-M4_MFD EPF RAMA2	3.34	0.76	1.00	9.12
OEN-1	0.60	0.61	0.67	7.98
OEN-10	1.28	0.06	0.06	1.25
OEN-11	1.13	0.88	0.94	11.22
OEN-12	1.88	0.58	0.65	8.10
OEN-2	5.21	0.90	1.11	12.27
OEN-3	3.62	1.08	1.33	14.51
OEN-4	2.59	0.79	0.94	10.43

Name	System pressure loss (bar)	Mixture velocity at inlet (m/s)	Mixture velocity at outlet (m/s)	Maximum erosion velocity ratio (%)
OEN-5	2.83	0.95	1.13	10.97
OEN-6	2.43	0.69	0.79	9.99
OEN-7	0.61	0.59	0.63	8.26
OEN-8	5.68	1.64	2.13	20.27
OEN-9	0.33	0.88	0.92	10.27
PTG BMD_MFD EPF RAMA2	25.69	3.14	10.95	56.79
RAA-2	6.09	0.09	0.13	1.05
RAA-5	5.78	0.05	0.06	0.77
SBEK-1	7.82	0.50	0.70	7.32
SOEN-1	5.58	0.03	0.03	0.61
WBEK-3	1.22	0.74	0.83	8.23
WOEN-2	2.72	1.10	1.28	13.45
WOEN-3	2.45	1.25	1.43	16.86
WOEN-4	4.45	0.27	0.33	4.59
WOEN-6	1.01	1.38	1.44	15.83
WOEN-7	6.33	0.37	0.47	6.90
WOENS-1	9.95	0.11	0.14	1.91
ZAM-1	6.27	0.56	0.82	7.22
ZAM2	0.93	0.81	0.90	9.18
ZMD-1	0.86	0.07	0.04	1.69

The optimization objective was to minimize pressure imbalance and reduce the maximum Erosion Velocity Ratio (EVR) across the network. Constraints included feasible multiphase velocities (1–5m/s), available commercial pipe diameters, and preservation of the existing network topology. Each candidate design was evaluated using the calibrated PIPESIM model.

Table 3. Current and modified pipeline diameters

Name	Current diameter	Optimized diameter
BEKN-1	6"	4"
BMDE-1	6"	4"
BMDN-1	6"	4"
BMDS-1	6"	4"
BMDSE-1	6"	4"
BMTG-1	6"	4"
BMTG-2	6"	4"
ERAA-2	6"	4"
HAS-1	6"	4"
HMGB-2	6"	4"
JCT OEN_MFD OEN-M3	6"	4"
MFD BEK-M1_MFD EPF RAMA2	12"	14"

Name	Current diameter	Optimized diameter
MFD BEKN_MFD EPF RAMA2	12"	14"
MFD OEN-M1_MFD BEKN	8"	6"
MFD OEN-M4_JCT OEN	8"	6"
MFD RAA-M5_Nvx MFD RAA-M4	10"	6"
MFD RAA-M6_MFD RAA-M5	8"	6"
NRAA-1	8"	6"
NRAA-2	6"	4"
NRAA4	6"	4"
OEN-1	6"	4"
OEN-10	6"	4"
OEN-12	6"	4"
OEN-6	6"	4"
OEN-7	6"	4"
PTG BMD_MFD EPF RAMA2	8"	10"
RAA-2	6"	4"
RAA-5	6"	4"
SBEK-1	6"	4"
SOEN-1	6"	4"
WBEK-3	6"	4"
WOEN-4	6"	4"
WOEN-7	6"	4"
WOENS-1	6"	4"
ZAM-1	6"	4"
ZMD-1	6"	4"

The newly proposed diameters, illustrated in Table 3, were incorporated into the previously calibrated model, and the network was re-simulated to validate the selected values. The updated results, summarized in Table 4 and illustrated in figure 3, demonstrate a clear improvement in flow velocity distribution across the network, confirming the effectiveness of the proposed design modifications.

Table 4. Optimization results of the RAMA & RAA network

Name	System pressure loss (bar)	Mixture velocity at outlet (m/s)	Maximum erosion velocity ratio (%)
BEKN-1	0.85	1.91	11.02
BMD-1	3.87	3.12	13.60
BMDE-1	2.99	1.96	12.63
BMDN-1	6.99	3.09	12.62
BMDS-1	4.74	3.09	12.62
BMDSE-1	3.27	3.08	12.62

Name	System pressure loss (bar)	Mixture velocity at outlet (m/s)	Maximum erosion velocity ratio (%)
BMTG-1	3.46	1.25	8.75
BMTG-2	6.05	1.97	10.38
BRM-1	2.36	1.04	8.96
ERAA-1	0.45	1.10	10.66
ERAA-2	2.42	1.21	10.55
HAS-1	19.78	1.15	6.39
HMGB-2	1.85	1.08	8.07
JCT OEN_MFD OEN-M3	2.69	1.10	8.98
JCT WBEK-1_MFD BEK-M1	10.96	1.14	11.61
JCT ZAM_MFD RAMA-M1	6.70	2.44	10.74
MFD BEK-M1_MFD EPF RAMA2	10.31	4.23	15.92
MFD BEK-M2_MFD BEK-M1	5.83	2.81	12.35
MFD BEKN_MFD EPF RAMA2	10.65	4.84	15.34
MFD OEN-M1_MFD BEKN	5.78	1.45	10.17
MFD OEN-M2_MFD BEK-M1	11.81	4.77	10.92
MFD OEN-M3_MFD BEKN	6.69	3.39	10.78
MFD OEN-M4_JCT OEN	7.24	1.28	6.72
MFD OEN-M5_MFD OEN-M3	2.95	1.05	8.80
MFD RAA-M5_Nvx MFD RAA-M4	8.23	2.00	9.11
MFD RAA-M6_MFD RAA-M5	1.01	1.58	4.42
MFD RAMA-M1_MFD EPF RAMA2	4.04	1.49	12.54
NRAA-1	2.45	1.10	4.39
NRAA-2	1.69	1.31	4.40
NRAA4	4.51	1.12	4.77
Nvx MFD RAA-M4_MFD EPF RAMA2	3.34	1.00	11.03
OEN-1	1.38	1.73	8.94
OEN-10	1.28	1.57	5.01
OEN-11	1.11	1.09	9.03
OEN-12	4.78	1.72	8.70
OEN-2	5.05	1.29	9.75
OEN-3	3.56	1.55	9.89
OEN-4	2.52	1.10	9.76
OEN-5	2.76	1.37	11.38
OEN-6	5.92	2.05	8.46
OEN-7	1.35	1.64	8.19
OEN-8	5.93	2.58	11.56
OEN-9	0.33	1.05	9.61

Name	System pressure loss (bar)	Mixture velocity at outlet (m/s)	Maximum erosion velocity ratio (%)
PTG BMD_MFD EPF RAMA2	12.81	3.96	19.30
RAA-2	5.60	1.12	12.39
RAA-5	5.69	1.12	7.17
SBEK-1	8.62	1.88	10.43
SOEN-1	5.55	1.08	5.65
WBEK-1	0.04	0.69	9.01
WBEK-2	3.93	1.65	11.96
WBEK-3	1.93	2.15	10.80
WOEN-2	2.64	1.49	10.24
WOEN-3	2.42	1.57	8.88
WOEN-4	4.45	0.82	7.49
WOEN-6	0.97	1.58	9.55
WOEN-7	8.08	1.16	7.11
WOENS-1	9.22	1.35	7.73
ZAM-1	8.79	1.85	11.29
ZAM2	0.93	0.90	9.83
ZMD-1	0.89	1.04	4.37

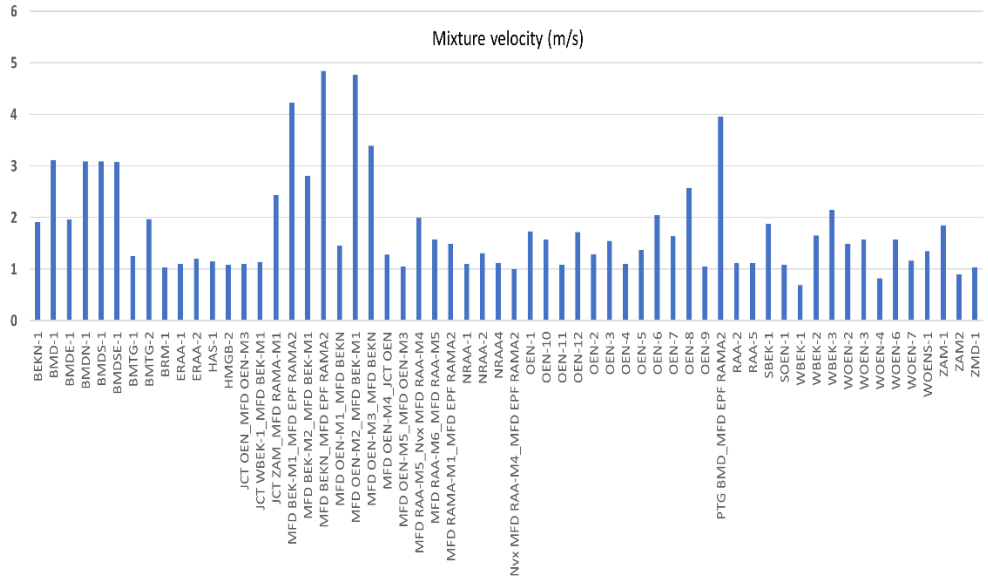

Figure 3. Histogram of mixture velocities after network optimization

While the optimized configuration performs well under the modeled conditions, it is important to recognize the practical limitations of the simulation approach.

The model is steady-state and does not capture transient thermal effects or short-term variations in flow behavior. These simplifications may slightly affect absolute pressure and velocity predictions when applied to real operating conditions. In practice, operational factors such as startup, shut-in, temperature fluctuations, and variations in (GOR) can produce temporary deviations from the steady-state baseline; however, these fluctuations occur around the modeled equilibrium, and therefore the relative optimization trends and the recommended network configuration remain valid.

CONCLUSIONS

The hydraulic modeling and optimization of the RAMA and RAA gathering network provided a comprehensive understanding of the system's flow behavior and performance. The calibration of the PIPESIM model demonstrated a strong agreement between simulated and measured pressures, with deviations below 7%, confirming the reliability of the constructed network model.

The initial analysis revealed several oversized and undersized flowlines, resulting in suboptimal flow velocities and high-pressure gradients in certain sections. The commissioning of new wells and the corresponding simulations highlighted an overall increase in pipeline and manifold pressures, emphasizing the importance of network reconfiguration to maintain balanced production.

Subsequent optimization efforts, including the adjustment of pipeline diameters and the integration of new flowlines, led to a more uniform velocity distribution across the network. The improved results, consistent with API design standards, confirm the technical soundness of the proposed modifications.

Overall, the optimized RAMA–RAA network model ensures safer operation, reduced erosion risk, and enhanced production efficiency, serving as a reliable framework for future development planning and well tie-in scenarios in the field.

EXPERIMENTAL SECTION

The modeling of the oil collection network for the RAMA and RAA fields was carried out using the PIPESIM 2022 software. This methodology describes the data acquisition, modeling procedure, and simulation steps performed to analyze flow behavior and optimize network performance.

Field Description and Data Collection

The RAMA and RAA production fields comprise 38 oil wells, of which 4 wells are shut-in. The total production of the active wells is approximately 407.9 m³/h of crude oil and 1.223.920 sm³/d of gas, transported to the EPF (Early Production Facility) RAMA-2 through a 109.5 km gathering network of various diameters. The main input data used for network modeling include well production parameters, pipeline geometry, collector characteristics, and fluid properties.

Reservoir Fluid Properties

The physical properties of the produced fluids are as follows: oil with a density of 43° API, gas with a density of 0.83, and water with a density of 1.02. The parameters measured during well testing include oil flow rate, gas flow rate, head and pipe pressures, temperature, and water cut (WC). The following relations are used to define two key parameters:

$$GOR = \frac{Q_g}{Q_h} \tag{2}$$

$$WC = \frac{Q_w}{Q_w + Q_h} \times 100 \tag{3}$$

where: Q_g is the gas flow rate. Q_h is the oil flow rate. and Q_w is the water flow rate.

Well Test Data

Table 5 presents the latest gauge data from the producing wells in the RAMA–RAA fields.

Table 5. Latest well gauge data

N°	Well	GOR	Qh (sm³/h)	Watercut (%)	T (C°)
01	BEKN1	155.21	0.9	0	35
02	BMD1	307.25	15	0	32
03	BMTG1	170	4.2	0	25
04	BMTG2	1941	8.1	29.67	29
05	BRM1	160.34	13.3	0	29
06	ERAA1	153.65	8.7	0	40
07	ERAA2	90.36	5.3	0	32
08	HAS1	81.85	1.8	0	40

N°	Well	GOR	Qh (sm^3/h)	Watercut (%)	T (C°)
09	HMGB2	74.75	13.3	0	32
10	NRAA1	19.5	2.8	0	45
11	NRAA2	20	8.4	0	37
12	NRAA4	27	2.9	0	29
13	OEN1	143.32	9.9	0	30
14	OEN10	33.6	3.1	0	36
15	OEN11	134.53	14.1	0	40
16	OEN12	121.89	10.7	0	35
17	OEN2	161.49	13.9	0	35
18	OEN3	167.76	16.1	0	25
19	OEN4	161.82	11.8	0	25
20	OEN5	168.1	10.8	0	30
21	OEN6	128.71	13.4	0	32
22	OEN7	121.58	11.5	0	32
23	OEN8	174.9	19.5	0	36
24	OEN9	152.66	11.8	0	30
25	RAA2	75.32	0.9	0	36
26	RAA5	96.5	1.1	57	25
27	SBEK1	136.46	8	0	26
28	SOEN1	39.39	1.3	0	33
29	SRAMA1	219	0.5	0	36
30	WBEK1	173.13	8.6	0	30
31	WBEK2	259.4	10.7	0	30
32	WOEN2	183.11	14.2	0	29
33	WOEN3	159.26	20.4	0	26
34	WOEN4	102.07	7	0	33
35	WOEN6	194.12	17.2	0	40
36	WOEN7	90.04	11.2	0	29
37	WOENS1	110.28	2.8	0	30
38	ZMD1	11	4.7	0	29

Pipeline and Collector Data

The gathering system consists of several flowlines and manifolds that transport the multiphase mixture of oil, gas, and water from the producing wells to the EPF RAMA-2 facility.

Table 6. Pipeline characteristics

Line name	Start	End	D (in)	L (m)	T (C°)
BEKN1 MFD BEKN	BEKEN1	MFD BEKEN	6"	1000	50
BMTG1 MFDBEK2	BMTG1	MFD BEK-M2	6"	3000	50
BRM1 MFD OEN2	BRM-1	MFD RAMA-1	6"	3499	50
ERAA2 MFD RAMA 1	ERAA-2	MFD RAMA-1	6"	2900	50
HAS1 MFDOEN4	HAS-1	MFD OEN-4	6"	14500	50
HMGB1 JCT ERAMA2	HMGB-1	JCT ERAMA-2	6"	7890	50
HMGB2 JCTZAM	HMGB-2	JCT ZAM	6"	2336	50
NRAA4 JCTNRAA1	NRAA-4	JCT NRAA-1	6"	5500	50
NRAA2 JCT NRAA1 8	NRAA-2	JCT NRAA-1	6"	5000	50
NRAA-1JCTNRAA-1 6	NRAA-1	JCT NRAA-1	8"	200	50
ERAA-3NV MFD4	ERAA-3	NVX MFD RAA4	6"	116	50
OEN1 JCT OEN 1	OEN-1	JCT OEN-1	6"	50	50
OEN4 MFD OEN3	OEN-4	MFD OEN-3	6"	3800	50
OEN5 MFD BEKN	OEN-5	MFD BEKN	6"	5400	50
OEN7 MFD OEN M5	OEN-7	MFD OEN-M5	6"	1500	50
OEN8 MFDBEKEN	OEN-8	MFD BEKN	6"	130	50
OEN9 MFD OEN1	OEN-9	MFD OEN-M1	6"	980	50
OEN12 MFD OEN3	OEN-12	MFD OEN-M3	6"	3800	50
OEN 2 MDFOEN3	OEN-2	MFD OEN-M3	6"	6462	50
OEN 3 MFDOEN3	OEN-3	MFD OEN-M5	6"	4460	50
OEN 6 MFD OEN 5	OEN-6	MFD OEN-M5	6"	4300	50
RAA1 MDF RAA2	RAA-1	MFD RAA-M2	4"	8900	50
RAA2 NV MFD RAA 4	RAA-2	NV MFD RAA-4	6"	7200	50
RAA5 NV MFD M4	RAA-5	NV MFD RAA-M	6"	6100	50
WBEK1 POINT BEK 1	WBEK-1	PNT BEK-1	6"	7480	50
WBEK2 MFDBEK2	WBEK-2	MFD BEK-M2	6"	3800	50
WOEN2 MDF OEN 3	WOEN-2	MFD OEN-M3	6"	3400	50
WOEN3 MFD OENM2	WOEN-3	MFD OEN-M2	6"	3200	50
WOEN4 MFD OEN M2	WOEN-4	MFD OEN-M2	6"	3267	50
WOEN5 MFD BEKEN	WOEN-5	MFD BEKN	6"	4200	50
WOEN6 MFDOENM2	WOEN-6	MFD OEN-M2	6"	3267	50

Table 7. Collector characteristics

Collector name	Start	End	D (in)	L(m)	T(C°)
JCT NRAA1 MFD RAA5	JCT NRAA-1	MFD RAA-M5	8"	17000	50
JCT OEN1 MFD OEN3	JCT OEN-1	MFD OEN-3	8"	4500	50
MDF RAA (M2 M3)12	MFD RAA-M2	MFD RAA-M3	12"	6426	50
MDF RAA (M2 M3)6	MFD RAA-M2	MFD RAA-M3	6"	6925	50
MDF RAA (M3 M4) A	MFD RAA-M3	MFD RAA-M4	8"	5184	50
MFD (OEN M1 BEKEN)	MFD OEN-M1	MFD BEKEN	8"	9800	50
MFD (OENM3 BEKEN)	MFD OEN-M3	MFD BEKEN	8"	8000	50
MFD (ZMD RAA-M5)	MFD ZMD	MFD RAA-M5	8"	13700	50
MFD BEK (M2 M1)	MFD BEK-M2	MFD BEK-M1	8"	9000	50
MFD BEK 1 PNT BEK 1	MFD BEK-M1	PNT BEK-1	6"	400	50
MFD BEKEN EPF RAMA 2	MFD BEKEN	EPF RAMA-2	12"	12000	50
MFD OEN 5 3	MFD OEN-5	MFD OEN-3	8"	6000	50
MFD OENM4 JCTOEN1	MFD OEN-M4	JCTOEN-1	8"	6500	50
MFD RAMA M1 EPF RAMA 2	MFD RAMA-M1	EPF RAMA-2	10"	17697	50
MFDRAA (M4 M3)	MFD RAA-M4	MFD RAA-M3	6"	6925	50
NV MFD RAA4 EPF RAMA2	NV MFD RAA-M4	EPF RAMA-2	12"	6000	50
PNTBEK1EPFRAMA B	PNT BEK-1	EPF RAMA-2	8"	19976	50
POINT BEK1 EPFRAMA2 A	PNT BEK-1	EPF RAMA-2	8"	16500	50
POINT ERRA-1 MFD RAA-1	PNT ERAA-1	MFD RAA-M1	8"	7200	50

Modeling Procedure

The digital model was constructed in PIPESIM by defining all components from source points (wells) to sinks (EPF RAMA-2). Simulations were performed using the PIPESIM steady-state multiphase flow simulator (Schlumberger, 2022), following an approach similar to that used in recent studies for multiphase flow modeling of wells and gathering networks [16-17]. The network includes wells, flowlines, junctions, and manifolds, with boundary conditions applied at both ends of the system. Fluid properties were defined using four possible methods available in PIPESIM: compositional model by specifying molar composition, PVT file based on laboratory measurements, MFL file (Multi-flash) for multi-phase definition, and black oil model defined by physical parameters (specific gravity API, viscosities. etc.). The model uses empirical correlations to predict pressure drops and flow regimes. The selected methods include the Beggs & Brill correlation [14], which tends to underestimate pressure losses in flowlines containing low points or liquid accumulation zones, and the Dukler-Eaton-Flannigan correlation [18] , which tends to overestimate losses in downhill sections without undulations. For each source (well), the following data were entered: oil flow rate, gas-oil ratio (GOR), temperature, and watercut. For each flowline and collector, the outer diameter (OD) and schedule, elevation profile as a function of length, and roughness factor were defined. The roughness factor was set to 0.0018 for

new pipelines and 0.004 for older lines. All simulations were performed in steady-state mode, which is appropriate for evaluating long-term hydraulic behavior and network optimization.The modeling workflow was developed using the PIPESIM multiphase flow simulator (Schlumberger, 2022). The sink node was defined by specifying the pressure at the arrival point (EPF RAMA-2). Heat transfer was considered using standard hydrocarbon parameters: pipe conductivity of 45 w/(m·k), burial depth of 0 inches (air-laid lines) or 31.5 inches (buried lines), and ambient temperature of 50°C (summer) and 5°C (winter). Fluid properties were assigned, including a light oil and gas mixture with density, viscosity, and API gravity defined. The correlation used for Pb (bubble point pressure) and Rs (solution gas ratio) is based on Glaso [19]. For Bo (oil formation volume factor), the Standing correlation is applied. The correlation used for oil viscosity is based on the methods of Petrosky et al. [20] Beal [21], or Pedersen [22], depending on the oil type and reservoir condition. After assembling the network, the model was run iteratively. The simulated values were compared with field measurements (pressure and flow rate). When discrepancies were found, calibration was performed by adjusting input parameters until the simulated and measured data matched satisfactorily. The calibration process ensured accurate prediction of pressure, temperature, and flow distribution across the network.

The final constructed model of the RAMA–RAA field network is shown in Figure 4, which provides a schematic representation of the overall topology of wells, manifolds, and gathering lines leading to the EPF RAMA-2 sink. The simulation results were based on this calibrated configuration.

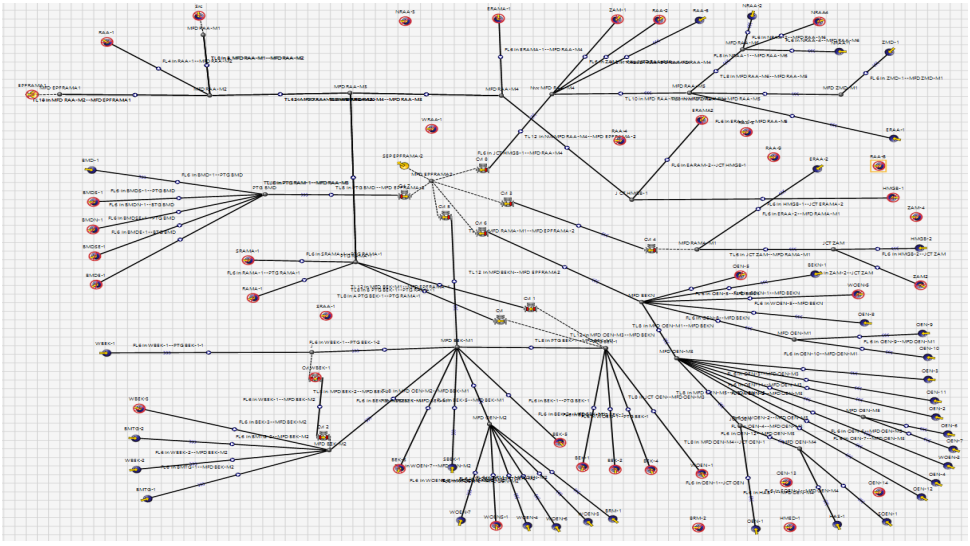

Figure 4. Network schematic of the RAMA–RAA field modeled in PIPESIM

ACKNOWLEDGMENTS

The authors express their sincere gratitude to the entire EP SONATRACH team for their kind support and valuable assistance, with special thanks to Mr. Lemiz Fatih and Mr. Boussandel Abdelaziz.

REFERENCES

1. F. Souas; A. Safri; A. Benmounah; *Pet. Sci. Technol*., **2020**, *38*, 849-857.
2. S. Pattanaik; U. Behera; D. Das; P. K. Misra; *J. Macromol. Sci. B*, **2025**, *64*, 586-604.
3. H. A. Abbas; A. D. Manasrah; L. Carbognani; K. O. Sebakhy; M. E. H. E. Nokab; M. Hacini; N. N. Nassar; *Pet. Sci. Technol*., **2022**, *40*, 1279-1301.
4. F. Souas; A. Safri; A. S. E. Meddour; *Studia UBB Chemia*., **2025**, *70*, 221-234.
5. F. Souas; A. Safri; A. Gueciouer; *Studia UBB Chemia*., **2025**, *70*, 177–190.
6. A. S. E. Meddour; F. Souas; Ovidius Univ. Ann. Chem., **2022**, *33*, 64–70.
7. R. Kumar; S. Banerjee; A. Banik; T. K. Bandyopadhyay; T. K. Naiya; *Pet. Sci. Technol*., **2017**, *35*, 615-624.
8. S. K. Das; M. N. Biswas; A. K. Mitra; *Chem. Eng. J*., **1991**, *45*, 165–171.
9. J.L. Trallero; *Oil-Water Flow Patterns in Horizontal Pipes*; Ph.D. Dissertation, The University of Tulsa: Tulsa, OK, USA, **1995**.
10. E. W. M. Hansen; *Emerg. Technol. Fluids Struct. Fluid-Struc. Interact*., **2001**, *431*, 23–29.
11. A. C. Bannwart; *J. Pet. Sci. Eng*., **2001**, *32*, 127–143.
12. T. K. Bandyopadyay; S. K. Das; *J. Pet. Sci. Eng*., **2007**, *55*, 156–166.
13. M. Rudman; H. M. Blackburn; *Appl. Math. Model*., **2004**, *30*, 1229–1248.
14. D. H. Beggs; J. P. Brill; *J. Pet. Technol*., **1973**, *25*, 607–617.
15. F. M. Sani; S. Huizinga; K.A. Esaklul; S. Nesic; *Wear*., **2019**, *426*, 620–636.
16. I. Ahmed; A. P. Iswara; S. Abbas; F. Q. Jamal; I. Ahmad; S. T. H. Shar; A. Naseem; *Heliyon*., **2024**, *10*, e35006.
17. M. Janadeleh; R. Ghamarpoor; N. K. Abbood; S. Hosseini; H. N. Al‐Saedi; A. Z. Hezave; *Heliyon*., **2024**, *10*, e36934.
18. A. E. Dukler; M. Wicks III; R. G. Cleveland; *AIChE J*., **1964**, *10*, 44–51.
19. O. Glaso; *J. Pet. Technol*., **1980**, *32*, 785–795.
20. G. E. Petrosky Jr; F. F. Farshad; *SPE Pap*., **1995**, SPE-29468.
21. C. Beal; *Trans. AIME*., **1946**, *165*, 94-115.
22. K. S. Pedersen; Å. Fredenslund; P. L. Christensen; P. Thomassen; *Chem. Eng. Sci*., **1984**, *39*, 1011–1016.